ENTPD3-specific CAR Regulatory T cells for Local Immune Control in T1D

Tom Pieper[1], Tobias Riet[1,2], Valerie Saetzler[1], Katharina Bergerhoff[3], Jenny McGovern[3], Louise Delsing[4], Mark Atkinson[5], Tracey Lodie[3], Lutz Jermutus[6], Fatih Noyan[1], Michael Hust [7], Irina Kusmartseva[5], Maike Hagedorn[1], Maren Lieber[1], Pierre Henschel[1], Viktor Glaser[1], Robert Geffers[8], Mingxing Yang[9], Julia Polansky-Biskup[9], Britta Eiz-Vesper[10], Agnes Bonifacius[10], Marc Martinez Llordella[3], Luke Henry[3], Daniela Penston[3], Artemis Gavriil[3], Thomas Grothier[3], Evanthia Nikolopoulou[3], Nikolaos Demertzis[3], Victoria Koullourou[3], Phillipa Cox[3], Bader Zarrouki[11], Marcella Sini[12], Janice Pfeiff[13], Isabelle Matthiesen[4], Matthias Hardtke-Wolenski[1,14*], Elmar Jaeckel[1,15*]

1 Hannover Medical School, Dept. of Gastroenterology, Hepatology, Infectious Diseases and Endocrinology, Hannover, Germany

2 University of Cologne, University Hospital of Cologne and Center for Molecular Medicine Cologne (CMMC), Department I of Internal Medicine, Tumor Genetics, Cologne, Germany

3 Quell Therapeutics Limited, London, UK

4 Cell & Gene Therapy Safety, Clinical Pharmacology & Safety Science, R&D, AstraZeneca, Gothenburg, Sweden

5 University of Florida, Dept. of Pathology, Immunology and Laboratory Medicine, Gainesville, USA

6 Research and Early Development, Cardiovascular, Renal and Metabolism, BioPharmaceuticals R&D, AstraZeneca, Cambridge, UK

7 Technische Universität Braunschweig, Dept. Medical Biotechnology, Braunschweig, Germany

8 Helmholtz Centre for Infection Research, Genome Analytics, Braunschweig, Germany

9 Berlin Institute of Health Center for Regenerative Therapies at Charité Universitätsmedizin Berlin, and German Rheumatology Research Centre, Immuno-Epigenetics, Berlin, Germany

10 Hannover Medical School, Institute of Transfusion Medicine and Transplant Engineering, Hannover, Germany

11 Bioscience Metabolism, Research and Early Development, Cardiovascular, Renal and Metabolism (CVRM), BioPharmaceuticals R&D, AstraZeneca, Gothenburg, Sweden

12 Discovery Imaging IBA, Clinical Pharmacology & Safety Science, R&D, AstraZeneca, Gothenburg, Sweden

13 Department of Pathology, Clinical Pharmacology & Safety Sciences, R&D, AstraZeneca, Gothenburg, Sweden

35 14 University of Duisburg-Essen, University Hospital Essen, Institute of Medical Microbiology,
36 Essen, Germany

37 15 University of Toronto, Center for Liver Transplantation, Center for Islet Transplantation,
38 Multi Organ Transplant Center, Toronto, Canada

39 *contributed equally

Abstract (146 words):

Despite advances in Type 1 Diabetes (T1D) management such a hybrid closed loop systems, patients still face significant morbidity, reduced life expectancy, and impaired glucose regulation compared to healthy individuals or those with pancreas transplants.

Here we developed beta cell-specific Chimeric Antigen Receptors (CAR) targeting the antigen ectonucleoside triphosphate diphosphohydrolase 3 (ENTPD3) using a novel cell-based phage display methodology. ENTPD3 is highly expressed on beta cells of both early and progressed T1D patients. ENTPD3 CAR regulatory T cells (Tregs) homed, expanded and persisted in pancreatic islets in a T1D mouse model (NOD) and completely prevented disease progression. Human ENTPD3 CAR Tregs displayed a stable regulatory phenotype, strong activation, and suppression. Importantly, ENTPD3 CAR T cells recognised and were fully activated by human islets.

This approach holds great promise as a durable treatment option for patients with prediabetes, new-onset diabetes, or those undergoing beta cell replacement therapy.

54 **Introduction (375 words):**

55 Patients diagnosed with Type 1 Diabetes (T1D) continue to face substantial challenges,
56 experiencing significant morbidity primarily attributable to the complications arising from
57 fluctuating blood glucose levels and overall see a reduction in life expectancy by a decade[1-3].

58 Although technological advancements, such as Continuous Glucose Monitoring (CGM)
59 sensors and hybrid closed-loop pumps, have improved glycaemic control, particularly during
60 nocturnal periods, they fall short of replicating the robust metabolic control achieved by
61 endogenous beta cells[4,5].

62 While pancreas, islet or stem cell derived beta cell transplantation offers a potential
63 biological replacement for beta cells, the associated challenges and risks, including immune
64 rejection and the need for systemic immunosuppression, underscore the demand for
65 innovative therapeutic approaches[6].

66 Disease modifying therapies and immune modulation strategies, particularly in the context
67 of new-onset T1D, have recently demonstrated success in clinical trials, albeit leading to only
68 transient preservation of minimally stimulated c-peptide responses[7,8].

69 Clinical trials administering polyclonal regulatory T cells (Tregs) in patients with T1D have
70 shown a good safety profile but limited efficacy[9,10]. Pre-clinical data has shown superiority of
71 antigen-specific Tregs over polyclonal Tregs in the NOD model of T1D and Tregs with beta
72 cell-specific T cell receptors (TCR) have shown promise in establishing prolonged local
73 tolerance in pre-clinical models[11-13] but challenges arising from Major Histocompatibility
74 Complex II (MHC II) polymorphism and the heterogeneity of immune responses in T1D
75 patients have hindered the development of a viable clinical product for over two decades.

76 Recent advancements in the use of Chimeric Antigen Receptor (CAR) Treg cells have
77 demonstrated success in achieving local immune control in murine and humanized mouse
78 models. MHC I A*02 specific CAR-Tregs, activated independently of MHC II restriction, exhibit
79 localized accumulation and prevented allograft rejection in mouse models and humanized
80 mice[14-16]. Ongoing clinical trials exploring the use of A2-CAR-Tregs in kidney and liver
81 transplantation provide a foundation for extending this approach to the context of T1D.

82 Herein, we identified ectonucleoside triphosphate diphosphohydrolase 3 (ENTPD3) as beta
83 cell specific target and have generated CARs directed against ENTPD3 using a novel phage
84 display approach. We provide evidence for the antigen-specific functionality and safety of
85 ENTDP3 CAR-Tregs *in vivo*, *in vitro* and *ex vivo*. Thus, ENTPD3-specific CAR Tregs offer a
86 potential avenue for achieving durable, targeted and pancreas-specific immune control in
87 patients with T1D.

88 **Results (1653 words):**

89 **ENTPD3 as a Potential Target for Islet-Specific CAR-Treg Therapies**

90 Previous attempts to develop CAR therapies targeting insulin, the most specific protein
91 associated with beta cells, were ineffective in preventing or treating T1D[17]. *In silico* research
92 suggested that ENTPD3, a surface protein, is highly expressed in both mouse and human
93 beta cells[18-20].

94 It is critical for potential therapeutic targets to be expressed at all stages of T1D
95 pathophysiology. We demonstrated by histological analysis of pancreatic samples from
96 patients at various stages of T1D, obtained through the nPOD (Network for Pancreatic Organ
97 Donors with Diabetes) consortium, that ENTPD3 is consistently co-expressed with insulin
98 across multiple stages of disease, from the autoantibody-positive stage to stage 3 (Fig. 1AB).
99 Notably, some expression was detected in non-beta cells, during established, long duration
100 T1D (Fig. 1A).

101 The protein expression of ENTPD3 was corroborated by a re-analysis of single-cell RNA
102 sequencing data from patients at different stages of T1D (Fig. 1C-E)[21], showing strong
103 expression in beta cells across both autoantibody-positive and overt T1D stages, and
104 notably, in delta cells as well. We confirmed specific expression of ENTPD3 in human
105 pancreatic islets by immunohistochemistry analysis of a wide panel of human tissues (Fig.
106 1F). Finally, we confirmed that in prediabetic and diabetic NOD mice, ENTPD3 was expressed
107 in islets, with minimal expression detected in surrounding ductal cells (Fig. 1G). These
108 findings indicate that the NOD mouse model is suitable for proof-of-concept testing of
109 ENTPD3-targeted CAR-Tregs.

110 **Generation of ENTPD3-Specific Single-Chain Variable Fragment (scFv) Binders via Protein-**
111 **Cell Based Phage Display**

112 Traditionally, CAR therapies have relied on a limited number of established monoclonal
113 antibodies[22]. In contrast, our approach sought to generate diverse scFv binders and assess
114 their functional properties. By employing human phage display libraries, we expedited the
115 translation of binders into human CARs for clinical trials without requiring murine-to-human
116 adaptation. Previous work from this lab has demonstrated that successful panning against
117 human peptide sequences can result in the selection of binders that cannot recognise intact
118 proteins on cell surfaces [23]. Consequently, we developed an assay that enriched scFv-phage
119 binders against correctly folded surface proteins on target cells (Suppl. Fig. 1A) using cell
120 sorting following rigorous pre-absorption and washing (Suppl. Fig. 2). This method produced
121 a diverse array of ENTPD3-specific binders (Fig. 2A). We also compared our novel strategy
122 with a classical protein-based panning approach. While a completely cell-based panning
123 approach on murine ENTPD3 yielded 8 % target-specific scFvs, a similar approach on human
124 ENTPD3 yielded only a single target-specific scFv. We refined our protocol by combining one
125 round of protein-based panning with two consecutive rounds of cell-based panning yielding
126 nearly 50% human ENTPD3-specific scFvs comprising a highly diverse repertoire of individual
127 scFvs.

128 We confirmed binding specificity using intact cells expressing ENTPD3 on the cell surface
129 (Fig. 2BC). Furthermore, murine ENTPD3-specific binders were shown to stain islets of
130 C57Bl/6 mice, confirming that selected binders could recognise ENTPD3 in the pancreas (Fig.
131 2D).

132 Interestingly, we were unable to identify binders that were cross-reactive for human and
133 murine ENTPD3 (Fig. 2BC), a finding likely attributed to the low sequence homology between
134 the human and murine extracellular domains (Suppl. Fig. 1B). Therefore, we continued with
135 different scFvs for either murine-specific ENTPD3 to perform proof-of-concept experiments
136 in NOD mice or human-specific ENTPD3 for further characterisation of human CAR Tregs,
137 respectively.

138 To rule out cross-reactivity with other membrane proteins, we screened the selected binders
139 against 5,500 human membrane proteins using a membrane proteome array, confirming
140 exclusive binding to ENTPD3 without cross-recognition of ENTPD1 or ENTPD2 (Fig. 2EF).
141 ENTPD3 is an ectonucleotidase involved in extracellular nucleotide and ATP hydrolysis and
142 thereby in purinergic signalling, and contributes to the regulation of insulin secretion[19,24].
143 Consequently, it was essential to demonstrate that our scFv binders did not interfere with
144 ENTPD3 enzymatic activity. We saw no evidence that scFv binding impaired ENTPD3
145 function, even when added at high concentrations (Fig. 2GH).

146 **Murine ENTPD3-Specific CARs are Activated upon Target Engagement and Prevent**
147 **Cyclophosphamide-Induced Diabetes *In Vivo***

148 Murine and human ENTPD3-specific CARs were constructed using either CD8
149 hinge/transmembrane domains or IgG hinge/CD4 transmembrane domains, the latter
150 featuring a mutated Fc receptor binding region to prevent nonspecific activation (Fig. 3AB).
151 These second-generation CARs included a CD3zeta activation domain and a CD28
152 costimulatory domain, which are optimal for Treg activation, as demonstrated by Levings
153 and colleagues[25]. The CARs were tested in T cell hybridomas where NFAT activation induced
154 eGFP expression via a minimal IL2 promoter (Suppl. Fig. 3A). CAR candidate m001 exhibited
155 strong target-specific activation without background signalling in both hinge formats (Fig.
156 3CD). Due to the ability of stimulation by cross-linking antibodies targeting Fab domain
157 candidate m001 in the long hinge format was selected for further analysis. This CAR was not
158 stimulated by the homolog ENTPD1 (Suppl. Fig. 3B). m001 also recognised MIN6 beta cells
159 (Suppl. Fig. 3CD) which were shown previously to express ENTPD3[19]. In murine CD4+ T cells,
160 ENTPD3-specific CARs stimulated target-dependent proliferation and activation (Fig. 3E,
161 Suppl. Fig. 4AB).

162 In a spontaneous diabetes NOD model where disease was synchronised by a single low-dose
163 cyclophosphamide injection, ENTPD3-specific CAR-T cells (m001) showed strong early
164 homing to pancreatic islets (day 3), unlike PE-specific control CAR-T cells (Fig. 3FG). In
165 contrast, ENTPD3-specific CAR-T cells (m001) were absent from pancreatic lymph nodes.
166 After 21 days, 15% of CD4+ cells in the pancreatic islets were ENTPD3 CAR-Tregs, reflecting a
167 combination of homing, expansion, and persistence (Suppl. Fig. 4C).

168 In the cyclophosphamide-induced T1D model (Fig. 3H), m001 CAR-Tregs prevented diabetes
169 onset, with no cases of T1D in the treatment group, compared to 50% incidence in control
170 animals (Fig. 3I). In this experiment, we confirmed that ENTPD3 CAR-Tregs persisted long-
171 term and were exclusively located in pancreatic islets (Fig. 3J). We observed no detectable
172 homing to off-target tissues such as the testes or colon, as confirmed by digital PCR (Fig. 3K).
173 Finally, murine ENTPD3 CAR-Tregs displayed a stable regulatory phenotype (Suppl. Fig. 5).

174 **Generation of Human CARs Recognising ENTPD3**

175 We deployed scFvs recognizing human ENTPD3 (Fig. 2B) to construct human CARs featuring
176 either CD8 hinge and CD28 transmembrane region or CH2CH3 hinge and CD28
177 transmembrane region and performed functional characterization in Jurkat cells expressing
178 luciferase under an NFAT-dependent minimal IL-2 promoter. Five CARs were identified that
179 exhibited strong activation with no tonic signalling in the absence of antigen (Fig. 4A).
180 Notably, CARs that strongly activated after recognising target cells over expressing ENTPD3
181 were also capable of recognising ENTPD3 on RT-4 cells, which endogenously express
182 ENTPD3.

183 The five CARs identified in the screening stage were transduced into human nTregs. In
184 activation assays using these cells, we observed robust upregulation of activation markers
185 CD69, CD137, and the Treg-specific marker GARP following activation by ENTPD3 (Fig. 4B-D),
186 with activation comparable to TCR stimulation. Coculture experiments of ENTPD3 expressing
187 B cells, allospecific T effector cells (Teff) and ENTPD3 CAR Tregs demonstrated that ENTPD3
188 CAR Tregs could be activated by B cells expressing ENTPD3 to cross-suppress CD4+ Teffs
189 activated by an TCR driven response to allogeneic B cells. This ability to control T cells with
190 different specificities is a crucial function of CAR-Tregs given the need to suppress T cells
191 reactive against various beta cell antigens within the islets (Fig. 4E). Importantly, CAR
192 transduction did not affect the stability of the regulatory phenotype, as evidenced by
193 sustained expression of CD25, FOXP3, CTLA-4, Helios and ICOS as shown for CAR candidates
194 h003 and h007 (Fig. 4F).

195 Second-generation CARs utilise partial activation motifs of the TCR complex, yet provide
196 CD28 costimulatory signals. We therefore compared human ENTDP3-specific CAR Tregs in
197 terms of CAR or TCR-based stimulation, focusing on the promising CAR candidate h003 more
198 closely. CAR stimulated h003 CAR Tregs produced comparable levels of IL-10, IL-8, and IL-17a
199 to those seen after TCR activation, with significantly increased TGF-β production (Fig. 5B).
200 CAR Treg phenotype was stable after both CAR and TCR stimulation indicative of high FOXP3
201 and CTLA4 expression, and activation marker GARP was upregulated (Fig. 5C). Epigenetic
202 demethylation of the TSDR region remained stable and indiscernible from untouched nTregs,
203 further confirming phenotypic stability (Fig. 5D)[26]. We further investigated the molecular
204 signalling pathways in CAR Tregs using RNA sequencing after CAR- and TCR-based activation.
205 Interestingly, critical Treg-associated genes, such as CD25, GARP, ICOS, and CTLA4, displayed
206 similar activation patterns, whereas LAG3, PD1 and TIGIT were more highly expressed after
207 CAR activation (Fig. 5E). While most genes were similarly regulated following TCR and CAR
208 stimulation, comparative cluster analysis identified genes uniquely upregulated following
209 CAR stimulation in cluster 2 (Fig. 5F), characterised by genes involved in IL-2 signalling and
210 NF-kB activation (Fig. 5G) and genes related to negative regulation of immune cells (Suppl.
211 Fig. 6). Additionally, further subtle differences in gene expression emerged as indicated by
212 pairwise comparison (Fig. 5H).

213 ***Ex vivo* Validation of Human ENTPD3 CAR Engagement and Activation**

214 Based on these functional characteristics, three CAR candidates were selected for
215 subsequent testing against human islets. Given the semi-quantitative nature of *in vitro* Treg
216 function assays, we further characterised ENTPD3 CARs in Teffs, as quantitative differences
217 *in vitro* activation may correlate with variations in *in vivo* activity[27]. Notably, human CD4+
218 and CD8+ T cells transduced with the ENTPD3 CAR exhibited strong antigen-specific
219 activation and proliferation (Suppl. Fig. 7)

220 As no relevant humanised T1D animal model exists, we were unable to test human ENTPD3
221 CAR Tregs *in vivo*. Instead, we assessed the capacity of ENTPD3 CAR T cells to detect and
222 interact with reaggregated human islets[28] (Fig. 6A), comparing them to preproinsulin-specific
223 CD8+ T cells[29] and HLA-A*02-specific CAR T cells. ENTPD3 CAR T cells displayed time-
224 dependent accumulation and invasion into the islets (Fig. 6B), leading to robust activation
225 indicated by TNF-α and IFN-γ production and near-total destruction of beta cells and their
226 function (Fig. 6CD). Remarkably, ENTPD3 CAR T cells exhibited stronger activation than both
227 preproinsulin-specific CD8+ T cells and A2-specific CAR T cells. These experiments
228 demonstrate that the amount of ENTPD3 on human beta cells and the signal transduction of
229 ENTPD3 CARs are sufficient to activate T cells to full effector functionality.

230 **Discussion (1611 words):**

231 Polyclonal Treg therapies have demonstrated safety and phenotypic stability in clinical trials
232 in T1D and after organ transplantation[9,10,30]. However, despite the excellent safety profile,
233 these therapies lack efficacy. In the context of T1D a potential explanation is the scarcity of
234 beta cell-specific Tregs within the natural repertoire, estimated at approximately one in a
235 million Treg cells[31]. This rarity severely limits their ability to control autoimmunity specifically
236 targeting pancreatic islets in T1D.

237 In contrast, studies dating back two decades have shown that Tregs specific to beta cell
238 antigens, recognised through their TCRs, are considerably more potent than polyclonal
239 Tregs. These antigen-specific Tregs can induce long-lasting local immune regulation,
240 effectively curing new-onset T1D in mouse models[11-13]. Despite these promising preclinical
241 results, translating this approach into the clinic has been impeded by the MHC II restriction
242 of TCRs, which limits their broader applicability.

243 The development of CARs, capable of MHC-independent antigen recognition, has
244 revolutionised the field of immunotherapy, particularly in oncology[22,27]. The success of CAR T
245 cells in recognising tumour antigens has laid the groundwork for adapting similar
246 technologies to regulatory T cells, with the goal of achieving local immune regulation in
247 autoimmune diseases and transplantation. Notably, CARs targeting mismatched HLA-A*02
248 molecules have demonstrated local immune control in transplantation models without the
249 need for systemic immunosuppression[14-16]. These promising findings have led to clinical
250 trials evaluating the efficacy of CAR Tregs in kidney and liver transplantation (LIBERATE
251 NCT05234190).

252 Our research identified ENTPD3 as a highly promising target for beta cell-specific CAR Tregs.
253 ENTPD3 is expressed at relatively high levels in pancreatic beta cells and is present across all
254 stages of T1D, from healthy individuals to patients with autoantibodies (aabs) and recent-
255 onset T1D. Notably, ENTPD3 is also expressed in surrounding delta cells, even in long-
256 standing T1D, suggesting a broad yet specific expression pattern that could be leveraged for
257 targeted immune regulation.

258 It has been shown by us and others that scFv generated by phage display can be efficiently
259 used in CAR studies[15,17,23,32,33]. However, these approaches deployed peptides and
260 recombinant proteins which neglects the fact that most CARs target proteins are expressed
261 on the cell membrane. Several attempts have been undertaken before to perform phage
262 display directly on cells, but exclusively for the generation of antibodies[34-37]. Therefore, we
263 established a novel phage display approach relying on scFv panning on cell lines expressing
264 the target ENTPD3 for superior CAR generation. This approach allowed us to screen for
265 binders specifically recognising properly folded ENTPD3 protein with high specificity. High
266 sensitivity in CARs targeting ENTPD3 may be critical for detecting cells with low ENTPD3
267 expression, particularly in the context of new-onset T1D, where the number of beta cells is
268 already severely reduced[27]. Furthermore, the use of human phage display libraries
269 eliminated the need for humanisation of the CAR constructs, streamlining the translational
270 pathway.

271 A significant challenge in CAR T cell therapy, particularly in oncology, has been the
272 occurrence of off-target effects, where CARs inadvertently recognise and attack non-target
273 tissues, leading to toxicities[38,39]. On-target/off-tumor effects are a also a common issue
274 observed in CAR T therapies [18,20]. Similar risks for ENTPD3 CAR Tregs to encounter their

275 antigen outside the islet microenvironment are considered very low, as ENTPD3 protein
276 expression is highly restricted to pancreatic islets. Even if they did, they would require local
277 IL-2 signals, which are typically only available at sites of immune activation. Moreover, any
278 off-islet activation of Tregs would be of significantly lower consequence compared to CAR
279 Teffs as CAR Tregs are not inflammatory drivers. The low risk of side effects from Treg therapy
280 is supported by data from clinical trials with large doses of polyspecific Tregs[9,10,30].
281 Nevertheless, we conducted comprehensive analyses using tissue microarrays and
282 membrane proteome profiling, which confirmed the restriction of membranous ENTPD3
283 expression to the pancreas. Moreover, we demonstrated that ENTPD3 CARs do not inhibit
284 the enzymatic activity of ENTPD3, thus reducing the risk of unintended consequences from
285 CAR binding to ENTPD3[18,20] in the pancreas.

286 Although low levels of ENTPD3 mRNA signals were detected in tissues such as the testes and
287 colon, tissue microarray data showed no correlation with protein expression. This finding
288 was corroborated by *in vivo* biodistribution studies, where ENTPD3 CAR Tregs predominantly
289 localised to pancreatic islets and the spleen. No significant signals were detected in the
290 testes, colon, or other tissues, even with highly sensitive digital PCR. Importantly, 15% of the
291 CD4+ cells within the islets were ENTPD3 CAR Tregs, indicating a strong preferential homing
292 and localisation to the target tissue.

293 Mechanistically, ENTPD3 CAR Tregs differ from TCR Tregs in their mode of action. While TCR
294 Tregs primarily interact with MHC II and antigen-presenting cells (APCs), CAR Tregs act
295 directly within the target tissue, such as the pancreatic islets. This distinction explains why
296 ENTPD3 CAR Tregs were exclusively found in the islets, whereas beta cell-specific TCR Tregs
297 also accumulate in the lymph nodes[13]. We show that suppression of immune responses by
298 ENTPD3 CAR Tregs occurs through cross-suppression of CD4+ Teffs with various antigen
299 specificities. This is particularly important in T1D, where the autoimmune response targets
300 multiple beta cell antigens.

301 The concept of cross-suppression is supported by a strong preventative effect of ENTPD3
302 CAR Tregs in the NOD mouse model, where autoimmune responses are caused by several
303 autoantigens. Similar results have been reported in transplantation models, where A2-CAR
304 Tregs, after being activated by the HLA-A*02 molecule, locally controlled all other T cell
305 responses against fully MHC-mismatched grafts[15]. Moreover, recent work by Levings et al.
306 demonstrated that local activation of CAR Tregs can lead to the conversion of beta cell
307 antigen-specific naïve T cells into Tregs[40], a phenomenon previously described as "infectious
308 tolerance" by Waldman et al[41]. This may explain the persistence of immune tolerance even
309 in the absence of tissue-specific Tregs in certain transplantation settings[42].

310 At the molecular level, transcriptome analysis revealed that ENTPD3 CAR Tregs exhibit
311 activation patterns similar to those of TCR-activated Tregs, particularly with respect to key
312 regulatory genes such as IL-10, TGF-β, CTLA-4, and CD25. Notably, activation via the CAR led
313 to increased expression of inhibitory receptors like LAG3, PD1, and TIGIT, as well as gene
314 clusters involved in IL-2 and NF-κB signalling. Despite this, ENTPD3 CAR Tregs did not exhibit
315 signs of exhaustion, which has only been reported in CARs with excessive tonic signalling[43].

316 There have been concerns that CAR Tregs might induce cytotoxicity[44,45]. However, our
317 experiments with ENTPD3-positive target cells, including HEK and B cells, did not show any
318 evidence of cell killing. This aligns with recent findings by Meyer et al., who reported that
319 ENTPD3 CAR Tregs do not induce cytotoxicity[45]. Furthermore, in the NOD model, metabolic

320 function remained stable despite a high local density of ENTPD3 CAR Tregs in the islets,
321 further supporting the non-cytotoxic nature of these cells.

322 Maintaining the stability of the human Treg phenotype is critical for ensuring that ENTPD3
323 CAR Tregs do not differentiate into proinflammatory effector cells. To mitigate this risk, we
324 used highly pure, sorted naïve Treg populations (CD127-, CD45RA+) to avoid contamination
325 with less stable Treg subsets, such as induced Tregs (iTregs)[46,47].

326 Our ENTPD3 CAR Tregs demonstrated stable demethylation of CpG residues in the Treg-
327 specific demethylated region (TSDR) and retained strong suppressive function[26].

328 To further increase safety of the human ENTPD3 CAR Tregs, we might improve the vector
329 design by including FOXP3 transgene in conjunction with the CAR. It has been reported that
330 overexpression of FOXP3 can drive enhanced Treg stability and suppressor function, even
331 under low IL-2 or inflammatory conditions[48,49]. Similar improvements were also observed
332 with increased IL-2 signalling through cis-acting membrane-bound IL-2[50].

333 We did not investigate alternative intracellular signalling domains for the CAR, as Levings et
334 al. have shown that the combination of CD3ζ and CD28 provides a sweet spot for optimal
335 Treg activation[25]. While constructs incorporating 4-1BB/ζ domains are used in cancer CAR
336 therapies to delay exhaustion and promote CAR T cell persistence, these configurations have
337 not been beneficial for Tregs[25,44].

338 Other beta cell-specific CAR targets, such as insulin[17] and tetraspanin 7[23], have been
339 explored, but none have demonstrated significant efficacy. A CAR recognising a
340 preproinsulin peptide in the context of I-A^{g7} successfully prevented diabetes development[51].
341 This approach rather mimics a TCR, but would not interfere with endogenous TCRs.
342 However, a human version of this CAR would be MHC-restricted and would require sufficient
343 doses of MHC/peptide complexes for activation. Thus, ENTPD3 CAR Tregs offer a more
344 versatile and non-MHC-restricted approach for achieving local immune control in T1D.

345 Our results are a significant step towards the clinical translation of ENTPD3 CAR Tregs for
346 T1D therapy. Large doses of polyclonal human Tregs have been demonstrated as safe in T1D
347 patients, with transferred cells maintaining a stable phenotype for over a year without
348 transitioning into effector cells[9]. The human ENTPD3 CAR has undergone extensive
349 characterisation, showing high functionality and specificity in recognising human islets.

350 This form of local immune control could be employed during stages 2 and 3 of T1D to
351 support endogenous beta cell regeneration. In long standing T1D, where beta cell
352 destruction is more extensive, ENTPD3 CAR Treg therapy could be combined with islet
353 transplantation, potentially reducing the need for systemic immunosuppression currently
354 required in trials involving stem cell-derived beta cells. Ideally, this therapy could be
355 administered as a single, long-lasting "living drug"[13], offering sustained immune regulation.

356 Innovative gene and cell therapies, like CAR Tregs are on the rise and might revolutionize the
357 way we combat graft rejection and autoimmune diseases in the near future. Clinical trials
358 will be necessary to determine the optimal cell dose and whether reapplication will be
359 required to sustain long-term tolerance. Here we introduced ENTPD3 CAR Tregs as a
360 promising approach to achieve tissue-specific tolerance without compromising systemic
361 immune competence paving the way for a novel treatment option in T1D.

Acknowledgements (186 words)

This work was supported by the ReSHAPE program, funded under the EU2020 program, with additional support from The Leona M. and Harry B. Helmsley Charitable Trust (2018PG-T1D06.3) and JDRF (3-SRA-2024-1529-S-B). Human CAR characterization was done in collaboration with Quell Therapeutics and Astra Zeneca. Quell Therapeutics supported the work at MHH as part of collaborative research support. Experiments with reaggregated human pseudoislets were done in collaboration with Quell Therapeutics and InSphero AG. This research was performed with the support of the Network for Pancreatic Organ Donors with Diabetes (nPOD), a collaborative type 1 diabetes research project funded by JDRF. Organ Procurement Organizations partnering with nPOD to provide research resources are listed at www.jdrfnpod.org/our-partners.php. The authors want to express their thank to Matthias Ballmaier of MHH's Central Research Facility Cell Sorting for supervision and support. Maximilian Fuchs of Fraunhofer Institute for Toxicology and Experimental Medicine (ITEM) for providing help in RNAseq data interpretation and to the Hannover Biomedical Research School (HBRS) for attending the PhD project of Tom Pieper. The PhD thesis of Tom Pieper and Master thesis of Viktor Glaser contains parts of the data published here.

Conflict of interest

TP, TR, MHW, MH and EJ are inventors on a patent application on antibodies against ENTPD3 and the corresponding CAR-Tregs. EJ is shareholder of Quell Therapeutics. JMcG, TL, MML, KB, LH, DP, AG, TG, EN, ND, VK, PC are officers of Quell Therapeutics and LD, LJ, BZ, MS, JP, IM are officers of Astra Zeneca.

385 **References**

386 1. Lind, M.*, et al.* Glycemic control and excess mortality in type 1 diabetes. *N Engl J Med*
387 **371**, 1972-1982 (2014).
388 2. Beck, R.W.*, et al.* The T1D Exchange clinic registry. *J Clin Endocrinol Metab* **97**, 4383-
389 4389 (2012).
390 3. Rawshani, A.*, et al.* Mortality and Cardiovascular Disease in Type 1 and Type 2
391 Diabetes. *N Engl J Med* **376**, 1407-1418 (2017).
392 4. Wadwa, R.P.*, et al.* Trial of Hybrid Closed-Loop Control in Young Children with Type 1
393 Diabetes. *N Engl J Med* **388**, 991-1001 (2023).
394 5. Choudhary, P.*, et al.* Advanced hybrid closed loop therapy versus conventional
395 treatment in adults with type 1 diabetes (ADAPT): a randomised controlled study.
396 *Lancet Diabetes Endocrinol* **10**, 720-731 (2022).
397 6. Reichman, T.*, et al.* Glucose-dependent insulin production and insulin-independence
398 in patients with type 1 diabetes infused with stem cell-derived, fully differentiated
399 islet cells (VX-880). in *EASD*, Vol. 66 (Suppl1) S229 (Diabetologia, Hamburg, 2023).
400 7. Herold, K.C.*, et al.* An Anti-CD3 Antibody, Teplizumab, in Relatives at Risk for Type 1
401 Diabetes. *N Engl J Med* **381**, 603-613 (2019).
402 8. Ramos, E.L.*, et al.* Teplizumab and beta-Cell Function in Newly Diagnosed Type 1
403 Diabetes. *N Engl J Med* **389**, 2151-2161 (2023).
404 9. Bluestone, J.A.*, et al.* Type 1 diabetes immunotherapy using polyclonal regulatory T
405 cells. *Sci Transl Med* **7**, 315ra189 (2015).
406 10. Marek-Trzonkowska, N.*, et al.* Administration of CD4+CD25highCD127- regulatory T
407 cells preserves beta-cell function in type 1 diabetes in children. *Diabetes Care* **35**,
408 1817-1820 (2012).
409 11. Tang, Q.*, et al.* In vitro-expanded antigen-specific regulatory T cells suppress
410 autoimmune diabetes. *J Exp Med* **199**, 1455-1465 (2004).
411 12. Tarbell, K.V., Yamazaki, S., Olson, K., Toy, P. & Steinman, R.M. CD25+ CD4+ T cells,
412 expanded with dendritic cells presenting a single autoantigenic peptide, suppress
413 autoimmune diabetes. *J Exp Med* **199**, 1467-1477 (2004).
414 13. Jaeckel, E., von Boehmer, H. & Manns, M.P. Antigen-specific FoxP3-transduced T-cells
415 can control established type 1 diabetes. *Diabetes* **54**, 306-310 (2005).
416 14. MacDonald, K.G.*, et al.* Alloantigen-specific regulatory T cells generated with a
417 chimeric antigen receptor. *J Clin Invest* **126**, 1413-1424 (2016).
418 15. Noyan, F.*, et al.* Prevention of Allograft Rejection by Use of Regulatory T Cells With an
419 MHC-Specific Chimeric Antigen Receptor. *Am J Transplant* **17**, 917-930 (2017).
420 16. Boardman, D.A.*, et al.* Expression of a Chimeric Antigen Receptor Specific for Donor
421 HLA Class I Enhances the Potency of Human Regulatory T Cells in Preventing Human
422 Skin Transplant Rejection. *Am J Transplant* **17**, 931-943 (2017).
423 17. Tenspolde, M.*, et al.* Regulatory T cells engineered with a novel insulin-specific
424 chimeric antigen receptor as a candidate immunotherapy for type 1 diabetes. *J*
425 *Autoimmun* **103**, 102289 (2019).
426 18. Docherty, F.M.*, et al.* ENTPD3 Marks Mature Stem Cell-Derived beta-Cells Formed by
427 Self-Aggregation In Vitro. *Diabetes* **70**, 2554-2567 (2021).
428 19. Syed, S.K.*, et al.* Ectonucleotidase NTPDase3 is abundant in pancreatic beta-cells and
429 regulates glucose-induced insulin secretion. *Am J Physiol Endocrinol Metab* **305**,
430 E1319-1326 (2013).

431 20. Saunders, D.C., *et al.* Ectonucleoside Triphosphate Diphosphohydrolase-3 Antibody
432 Targets Adult Human Pancreatic beta Cells for In Vitro and In Vivo Analysis. *Cell*
433 *Metab* **29**, 745-754 e744 (2019).
434 21. Fasolino, M., *et al.* Single-cell multi-omics analysis of human pancreatic islets reveals
435 novel cellular states in type 1 diabetes. *Nat Metab* **4**, 284-299 (2022).
436 22. Posey, A.D., Jr., Young, R.M. & June, C.H. Future perspectives on engineered T cells for
437 cancer. *Trends Cancer* **10**, 687-695 (2024).
438 23. Pieper, T., *et al.* Generation of Chimeric Antigen Receptors against Tetraspanin 7. *Cells*
439 **12**(2023).
440 24. Lavoie, E.G., *et al.* Identification of the ectonucleotidases expressed in mouse, rat,
441 and human Langerhans islets: potential role of NTPDase3 in insulin secretion. *Am J*
442 *Physiol Endocrinol Metab* **299**, E647-656 (2010).
443 25. Dawson, N.A.J., *et al.* Functional effects of chimeric antigen receptor co-receptor
444 signaling domains in human regulatory T cells. *Sci Transl Med* **12**(2020).
445 26. Polansky, J.K., *et al.* DNA methylation controls Foxp3 gene expression. *Eur J Immunol*
446 **38**, 1654-1663 (2008).
447 27. Hamieh, M., Mansilla-Soto, J., Riviere, I. & Sadelain, M. Programming CAR T Cell
448 Tumor Recognition: Tuned Antigen Sensing and Logic Gating. *Cancer Discov* **13**, 829-
449 843 (2023).
450 28. Yesildag, B., *et al.* Liraglutide protects beta-cells in novel human islet spheroid models
451 of type 1 diabetes. *Clin Immunol* **244**, 109118 (2022).
452 29. Skowera, A., *et al.* beta-cell-specific CD8 T cell phenotype in type 1 diabetes reflects
453 chronic autoantigen exposure. *Diabetes* **64**, 916-925 (2015).
454 30. Sawitzki, B., *et al.* Regulatory cell therapy in kidney transplantation (The ONE Study):
455 a harmonised design and analysis of seven non-randomised, single-arm, phase 1/2A
456 trials. *Lancet* **395**, 1627-1639 (2020).
457 31. Serr, I., *et al.* Type 1 diabetes vaccine candidates promote human Foxp3(+)Treg
458 induction in humanized mice. *Nat Commun* **7**, 10991 (2016).
459 32. De Paula Pohl, A., *et al.* Engineered regulatory T cells expressing myelin-specific
460 chimeric antigen receptors suppress EAE progression. *Cell Immunol* **358**, 104222
461 (2020).
462 33. Yoon, J., *et al.* FVIII-specific human chimeric antigen receptor T-regulatory cells
463 suppress T- and B-cell responses to FVIII. *Blood* **129**, 238-245 (2017).
464 34. Jones, M.L., *et al.* Targeting membrane proteins for antibody discovery using phage
465 display. *Sci Rep* **6**, 26240 (2016).
466 35. Min, B., *et al.* Semi-Automated Cell Panning for Efficient Isolation of FGFR3-Targeting
467 Antibody. *Int J Mol Sci* **22**(2021).
468 36. Yuan, Q.A., Robinson, M.K., Simmons, H.H., Russeva, M. & Adams, G.P. Isolation of
469 anti-MISIIR scFv molecules from a phage display library by cell sorter biopanning.
470 *Cancer Immunol Immunother* **57**, 367-378 (2008).
471 37. Lipes, B.D., *et al.* An entirely cell-based system to generate single-chain antibodies
472 against cell surface receptors. *J Mol Biol* **379**, 261-272 (2008).
473 38. Ghilardi, G., *et al.* T cell lymphoma and secondary primary malignancy risk after
474 commercial CAR T cell therapy. *Nat Med* **30**, 984-989 (2024).
475 39. Bonifant, C.L., Jackson, H.J., Brentjens, R.J. & Curran, K.J. Toxicity and management in
476 CAR T-cell therapy. *Mol Ther Oncolytics* **3**, 16011 (2016).
477 40. Wardell, C.M., *et al.* Short Report: CAR Tregs mediate linked suppression and
478 infectious tolerance in islet transplantation. *bioRxiv* (2024).

479 41. Cobbold, S. & Waldmann, H. Infectious tolerance. *Curr Opin Immunol* **10**, 518-524
480 (1998).
481 42. Lee, K., Nguyen, V., Lee, K.M., Kang, S.M. & Tang, Q. Attenuation of donor-reactive T
482 cells allows effective control of allograft rejection using regulatory T cell therapy. *Am J*
483 *Transplant* **14**, 27-38 (2014).
484 43. Lamarche, C.*, et al.* Tonic-signaling chimeric antigen receptors drive human regulatory
485 T cell exhaustion. *Proc Natl Acad Sci U S A* **120**, e2219086120 (2023).
486 44. Boroughs, A.C.*, et al.* Chimeric antigen receptor costimulation domains modulate
487 human regulatory T cell function. *JCI Insight* **5**(2019).
488 45. Wu, X.*, et al.* CD39 delineates chimeric antigen receptor regulatory T cell subsets with
489 distinct cytotoxic & regulatory functions against human islets. *Front Immunol* **15**,
490 1415102 (2024).
491 46. Liu, W.*, et al.* CD127 expression inversely correlates with FoxP3 and suppressive
492 function of human CD4+ T reg cells. *J Exp Med* **203**, 1701-1711 (2006).
493 47. Sakaguchi, S., Vignali, D.A., Rudensky, A.Y., Niec, R.E. & Waldmann, H. The plasticity
494 and stability of regulatory T cells. *Nat Rev Immunol* **13**, 461-467 (2013).
495 48. McGovern, J., Holler, A., Thomas, S. & Stauss, H.J. Forced Fox-P3 expression can
496 improve the safety and antigen-specific function of engineered regulatory T cells. *J*
497 *Autoimmun* **132**, 102888 (2022).
498 49. Henschel, P.*, et al.* Supraphysiological FOXP3 expression in human CAR-Tregs results
499 in improved stability, efficacy, and safety of CAR-Treg products for clinical application.
500 *J Autoimmun* **138**, 103057 (2023).
501 50. Kremer, J.*, et al.* Membrane-bound IL-2 improves the expansion, survival, and
502 phenotype of CAR Tregs and confers resistance to calcineurin inhibitors. *Front*
503 *Immunol* **13**, 1005582 (2022).
504 51. Spanier, J.A.*, et al.* Tregs with an MHC class II peptide-specific chimeric antigen
505 receptor prevent autoimmune diabetes in mice. *J Clin Invest* **133**(2023).
506

507 **Figure legends**

508 **Figure 1:** *ENTPD3 as potential target for islets-specific CAR-Treg therapies* **(A)** Human
509 pancreatic sections (nPOD) of individuals with different disease progression (Single
510 Autoantibody positive: AAb+ (S); Multiple Autoantibody positive: AAb+ (M); Early and late
511 T1D) were stained with anti-ENTPD3 antibody (red). Insulin (green) and glucagon (blue) were
512 co-stained. Non-diabetic sample served as control. **(B)** Quantification of islets staining for
513 ENTPD3. Left: Number of beta cells (Insulin+). Right: Percentage of beta cells expressing
514 ENTPD3. n per condition = 3-6. **(C-E)** ENTPD3 expression of human pancreatic cells of nPOD
515 samples. **(C)** UMAP visualization of cellular clusters of human pancreatic islets. (D) UMAP
516 visualizations of ENTPD3 expression in islets cells of healthy (Control), autoantibody-positive
517 (AAB) and T1D individuals (T1D). **(E)** Quantification of D. Dot size resembling percent of cells
518 expressing ENTPD3 within cell cluster. Colours indicating average expression strength. **(F)**
519 Tissue micro array (TMA) of different human organs stained for ENTPD3 (brown) show that
520 membranous ENTPD3 expression is highly specific to pancreatic islets. Hematoxylin
521 counterstain in blue. **(G)** Pancreatic sections of healthy and diabetic NOD mice were stained
522 for ENTPD3 (brown) and counterstained with hematoxylin (blue).

523 **Figure 2:** *Generation of ENTPD3-specific scFv binders by protein- and cell-based phage*
524 *display* **(A)** Outcome of scFv binders by different panning strategies for murine ENTPD3 and
525 human ENTPD3. Total number of analysed scFv binders per strategy are given in the centre of
526 each plot. Proportions of unique scFv clones (color-coded) and non- and unspecific binders
527 (grey). **(B-C)** Binding of human **(B)** and murine **(C)** ENTPD3-specific scFv binders was
528 measured by flow cytometry on human or murine ENTPD3 expressing HEK293T cells,
529 respectively. ENTPD3 expression on HEK cells was reported by coexpression of eGFP.
530 Representative plots of selected binders. **(D)** Staining of C57BL/6 pancreatic sections by
531 murine ENTPD3-specific binder m001. Insulin-specific FITC-conjugated antibody was used as
532 positive control (left). Incubation with scFv m001 was followed by FITC-conjugated secondary
533 antibody (right). Staining only secondary antibody served as negative control (middle). **(E)**
534 Membrane Proteome Array (MPA) screening was performed by testing of human ENTPD3
535 binders. Binding values are given for clones h003 and h007 in an scFv-Fc format for 5,372
536 distinct human membrane protein clones. **(F)** Binding values of MPA for ENTPD3 and 10
537 following proteins with highest values and ENTPD1 and ENTPD2. **(G-H)** ENTPD3 enzymatic
538 activity in the presence of soluble ENTPD3, ADP and scFv-Fc of h003 or h007. ENTPD3
539 activity (PO_4 formation) was measured by malachite green phosphate assay. Measured in
540 triplicates. **(G)** Phosphate formation up top 30 min after incubation with 3.3 nM ENTPD3-
541 specific scFv-Fc. No CAR and control CAR served as control. (H) Phosphate formation after
542 incubation with varying concentrations (100 – 1 nM) of ENTPD3-specific scFv-Fc. Additionally,
543 incubation with EDTA served as positive control for ENTPD3 inhibition. Data are presented as
544 mean ± SD of triplicates. p values determined by two-way ANOVA of h003, h007 and Control
545 CAR conditions, respectively. ns: $P > 0.05$.

546 **Figure 3:** *Murine ENTPD3-specific CAR are functionally stimulated upon target contact and*
547 *prevent cyclophosphamide-induced diabetes in vivo* **(A)** Design of murine CD8-derived hinge
548 CARs (short) and Fc-IgG-derived hinge CARs (long), containing a FOXP3 expression cassette
549 separated by P2A cleavage side, and reporter gene Thy1.1 (CD90.1) under control of an IRES.
550 **(B)** Illustration of both CAR constructs as expressed on the cell surface. **(C)** Representative
551 plots of stimulation of m001 in short and long hinge CAR format, respectively, in NFAT-GFP
552 reporter cell line. CAR stimulation shown as NFAT-controlled GFP expression and CAR

553 expression shown as anti-Fab antibody AF647 staining. **(D)** Screening of further murine
554 ENTPD-specific candidates for CAR stimulation in the aforementioned system. **(E)**
555 Proliferation of CAR T cells measured as dilution of CFSE signal. CFSE labelled murine CD4+
556 CAR T cells (mL-m001 or Control (PE-specific) CAR) were stimulated on mENTPD3 or control
557 antigen PE, or by aCD3/CD28 bead stimulus. Counts normalized to mode. Red: Stimulated
558 CAR T cells (of CD69+ Thy1.1+). Blue: Unstimulated cells (of CD69- Thy1.1-). Left:
559 Representative histograms. Right: Quantification of % Proliferation of stimulated CAR T cells
560 (of CD69+ Thy1.1+). Mean ± SD, triplicates. p values determined by two-way ANOVA and
561 multiple comparison testing (Tukey's test). **(F)** Schematic overview of setup for CAR T cell
562 homing experiment in NOD mice. **(G)** Comparison of biodistribution of m001 and Control
563 (PE-specific) CAR Teffs. CD4+ populations were analysed for percentage of Thy1.1+ cells. Data
564 are presented as mean ± SD. n=3 per group. p values determined by two-way ANOVA and
565 multiple comparison testing (Tukey's test). **(H)** Schematic overview of experimental setup for
566 prevention of cyclophosphamide-induced diabetes in NOD mice. **(I)** Diabetes-free individuals
567 over the course of the experiment. n=12 per group. Data from 8 independent experiments. p
568 value determined by log-rank test for m001 CAR cTreg compared to Control (PE-specific) CAR
569 cTreg and cyclophosphamide-only treated animals. **(J)** Comparison of biodistribution of m001
570 CAR-cTregs and Control (PE-specific) CAR cTregs at experimental endpoints (n = 3-6 per
571 group). Data are presented as mean ± SD of Thy1.1+ in the CD4+ population. p values
572 determined by two-way ANOVA and multiple comparison testing (Tukey's test). **(K)**
573 Biodistribution of m001 CAR Tregs in ENTPD3-expressing tissues by digital PCR. Organs of
574 two mice per group were saved at experimental endpoints and total gDNA was analysed by
575 digital PCR. Copy numbers of CAR Treg-specific WPRE sequence per µg gDNA are displayed. P
576 values for all experiments * P < 0.033, ** P < 0.002, *** P < 0.001.

577 **Figure 4:** *Human ENTPD3-specific CAR Tregs are functional and maintain Treg phenotype and*
578 *suppressive function* **(A)** NFAT luciferase Jurkat cell line was transduced with CARs comprising
579 different human ENTPD3-specific scFv (h003, h007, h008, h002 and h006). After 5 days cells
580 were activated with human ENTPD3 extracellular domain peptide, cell lines expressing
581 ENTPD3 (RT-4 and ENTPD3.HEK293T) at indicated ratios or left unstimulated. Activation of
582 cells was determined by luminescence measurement. Heatmap shows relative activation
583 levels in response to stimulus. Black represents the lowest levels of activation with red/pink
584 showing highest levels of activation. Representative of 3 separate experiments. **(B-D)** Human
585 ENTPD3 CAR Tregs were co-cultured with ENTPD3 extracellular domain, ENTPD3 expressing
586 HEK293T cells, RT-4, EndoBH5 cells or controls (aCD3/aCD28 beads, WT HEK293T and no
587 stimulation). After 24h activation markers CD69 **(B)**, CD137 **(C)** and GARP **(D)** were assessed
588 by flow cytometry. Mean ± SD of n=6 donors. p values determined by two-way ANOVA and
589 multiple comparison testing (Tukey's test). (**E)** CAR Tregs were co-cultured with WT B cell
590 line, ENTPD3 expressing B cell line or aCD3/28 beads and decreasing numbers of CTV-
591 labelled CD4+ Teffs for 5 days. Cells were assayed by flow cytometry and proliferation of Teffs
592 was determined by CTV dilution. Graphs show percentage suppression by ENTPD3 CARs and
593 mock transduced cells. Percentage suppression was calculated by normalizing proliferation of
594 Teffs stimulated in the presence of Tregs to Teffs alone. Data are presented as mean ± SD of
595 n=4-5 donors. p values determined by two-way ANOVA of B cells ENTPD3 and B cells WT
596 conditions, respectively. **(F)** h003 and h007 CAR Tregs were collected and stained by flow
597 cytometry for indicated markers. Percentage of each marker shown from the total CD4
598 population for Mock Tregs or gated on CAR+ cells for the CAR Tregs. Mean ± SD of n=8
599 donors. P values for all experiments * P < 0.033, ** P < 0.002, *** P < 0.001.

600 **Figure 5.** *ENTPD3 CAR Tregs (candidate h003) maintain Treg-specific phenotype and gene*
601 *expression upon stimulation* **(A)** Schematic overview and design of human CAR Treg
602 stimulation assay containing TSDR, transcriptomics and phenotype markers and cytokine
603 secretion readouts for testing of CAR h003. **(B)** Treg cytokine profile upon CAR and TCR-
604 dependent stimulation. ENTPD3 CAR Treg cells were incubated with ENTPD3, PE (control
605 antigen) or aCD3/CD28 beads. Cytokine concentration was determined by cytokine bead
606 array. Data are presented as mean ± SD of n=6 donors. p values determined by two-way
607 ANOVA and multiple comparison testing (Tukey's test). **(C)** Expression of Treg phenotype and
608 activation markers FOXP3, GARP and CTLA4 upon stimulation measured by flow cytometry.
609 ENTPD3-specific h003 CAR Tregs stimulated by aCD3/CD28 beads (black), ENTPD3 (orange)
610 or unrelated control antigen (blue). Data presented as mean ± SD of 4-6 donors. p values
611 determined by two-way ANOVA and multiple comparison testing (Tukey's test). **(D)** Analysis
612 of demethylation status of Treg-specific demethylated regions (TSDR). Percentage of
613 demethylation of different TSDRs is shown for ENTPD3 CAR Tregs (h003), Control (PE-
614 specific) CAR Tregs, nTregs and Teffs. Mean of data from 3 donors. **(E)** Gene expression of
615 Treg phenotype and activation genes upon stimulation of h003 CAR Tregs measured by RNA
616 Sequencing. Black: TCR-dependent stimulation by aCD3/CD28 beads. Orange: CAR-specific
617 stimulation by ENTPD3. Blue: Unrelated control antigen. Data mean ± SD of 3 donors. p
618 values determined by two-way ANOVA and multiple comparison testing (Tukey's test). **(F)**
619 Cluster analysis of transcriptome data. Z-score (color coded) shown for TCR-dependent
620 stimulation by aCD3/CD28 beads, CAR-specific stimulation by ENTPD3 and unstimulated
621 (unrelated control antigen). Data of 3 donors per condition. **(G)** Analysis of Human Molecular
622 Signatures Database (MSigDB) Hallmark gene sets of major clusters 1, 2 and 3. Size of dots
623 represent ratio of represented genes within each cluster. P value is color coded. **(H)** Volcano
624 plot of differentially expressed genes in pairwise comparison of CAR- (ENTPD3) and TCR-
625 (aCD3/CD28 beads) specific stimulation. p values for all experiments * $P < 0.033$, ** $P <$
626 0.002, *** $P < 0.001$.

627 **Figure 6:** *ENTPD3 CARs interact with human islets micro tissue (hIsMT) spheroids* **(A)**
628 Schematic assay setup. **(B)** Human CD8+ T cells expressing either ENTPD3 CARs (h003, h007
629 or h008) or HLA-A2 CAR, and GFP reporter cassette were co-cultured with hIsMT spheroids
630 for live imaging. Images show the hIsMT alone, with non-transduced CD8 T cells (Mock),
631 preproinsulin (PPI) specific cytotoxic lymphocytes (CTLs) or CD8 T cells expressing HLA-A2
632 CAR or ENTPD3 CARs h003, h007 or h008 for timepoints 0, 24, 48 and 72 h. T cells are shown
633 in red, CAR expression is shown in green and hIsMT are stained cyan. **(C)** After 48 h samples
634 of co-cultures were lysed and stimulated insulin secretion (left) and total content (right) was
635 determined by ELISA. Individual dots are technical replicates. Bars represent mean ± SD of
636 n=4-6 **(D)** After 72 h supernatants were collected and assayed for IFN-γ (left) and TNF-
637 α (right). Individual dots are technical replicates. Bars represent mean ± SD of n=6. p values
638 determined by One-way ANOVA with Dunnett's multiple comparisons test comparing all
639 conditions to mock CD8 T cells. Outliers were be detected with ROUT's outlier test (Q=5%).
640 *$p < 0.05$, **$p < 0.01$, ***$p < 0.001$.

ENTPD3-specific CAR Regulatory T cells for Local Immune Control in T1D

2024

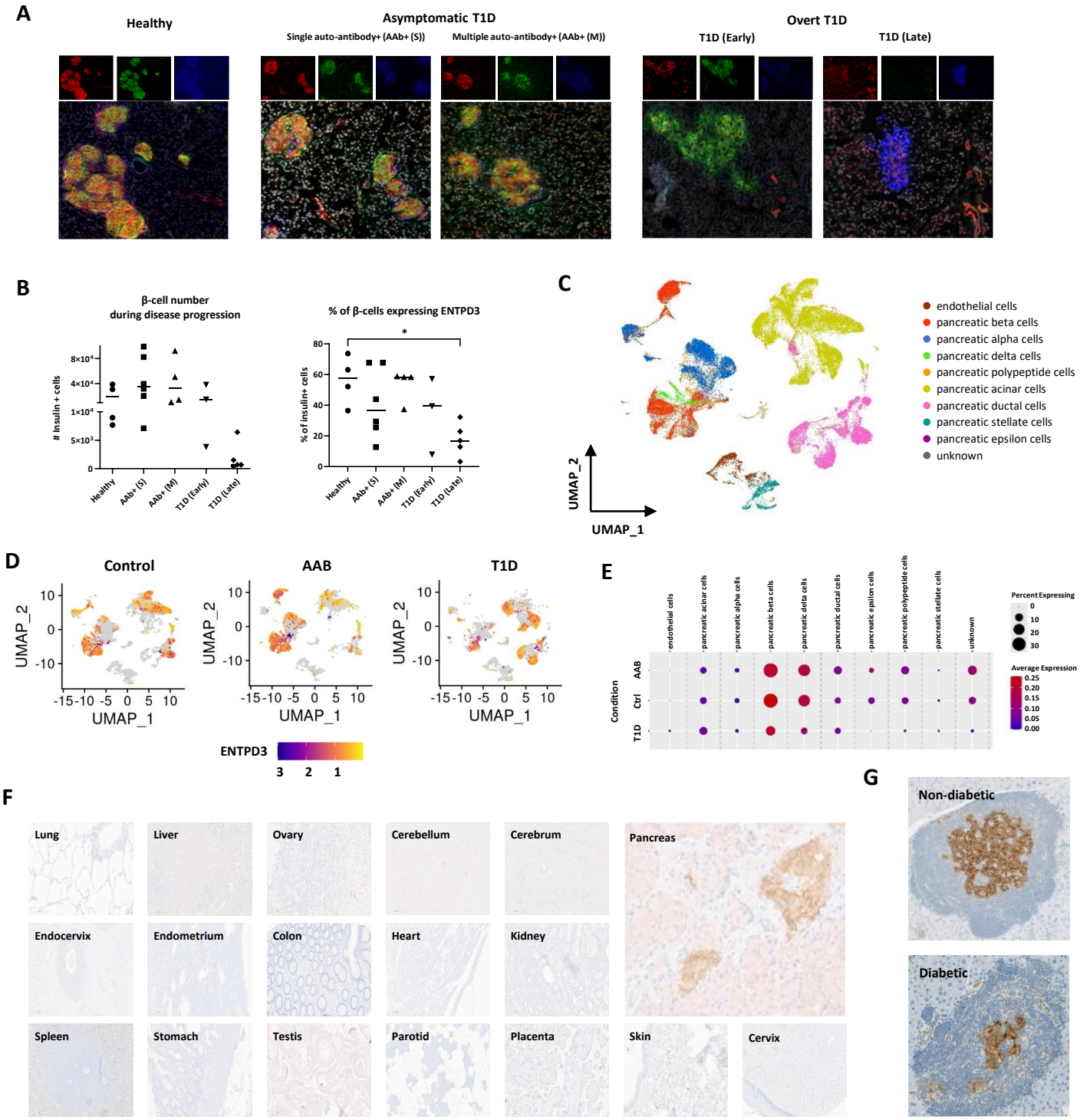

Figure 1: *ENTPD3 as potential target for islets-specific CAR-Treg therapies* **(A)** Human pancreatic sections (nPOD) of individuals with different disease progression (Single Autoantibody positive: AAb+ (S); Multiple Autoantibody positive: AAb+ (M); Early and late T1D) were stained with anti-ENTPD3 antibody (red). Insulin (green) and glucagon (blue) were co-stained. Non-diabetic sample served as control. **(B)** Quantification of islets staining for ENTPD3. Left: Number of beta cells (Insulin+). Right: Percentage of beta cells expressing ENTPD3. n per condition = 3-6. **(C-E)** ENTPD3 expression of human pancreatic cells of nPOD samples. (C) UMAP visualization of cellular clusters of human pancreatic islets. (D) UMAP visualizations of ENTPD3 expression in islets cells of healthy (Control), autoantibody-positive (AAB) and T1D individuals (T1D). (E) Quantification of D. Dot size resembling percent of cells expressing ENTPD3 within cell cluster. Colours indicating average expression strength. **(F)** Tissue micro array (TMA) of different human organs stained for ENTPD3 (brown) show that membranous ENTPD3 expression is highly specific to pancreatic islets. Hematoxylin counterstain in blue. Pancreas in 40x resolution, remaining organs in 20x resolution, respectively. **(G)** Pancreatic sections of healthy and diabetic NOD mice were stained for ENTPD3 (brown) and counterstained with hematoxylin (blue).

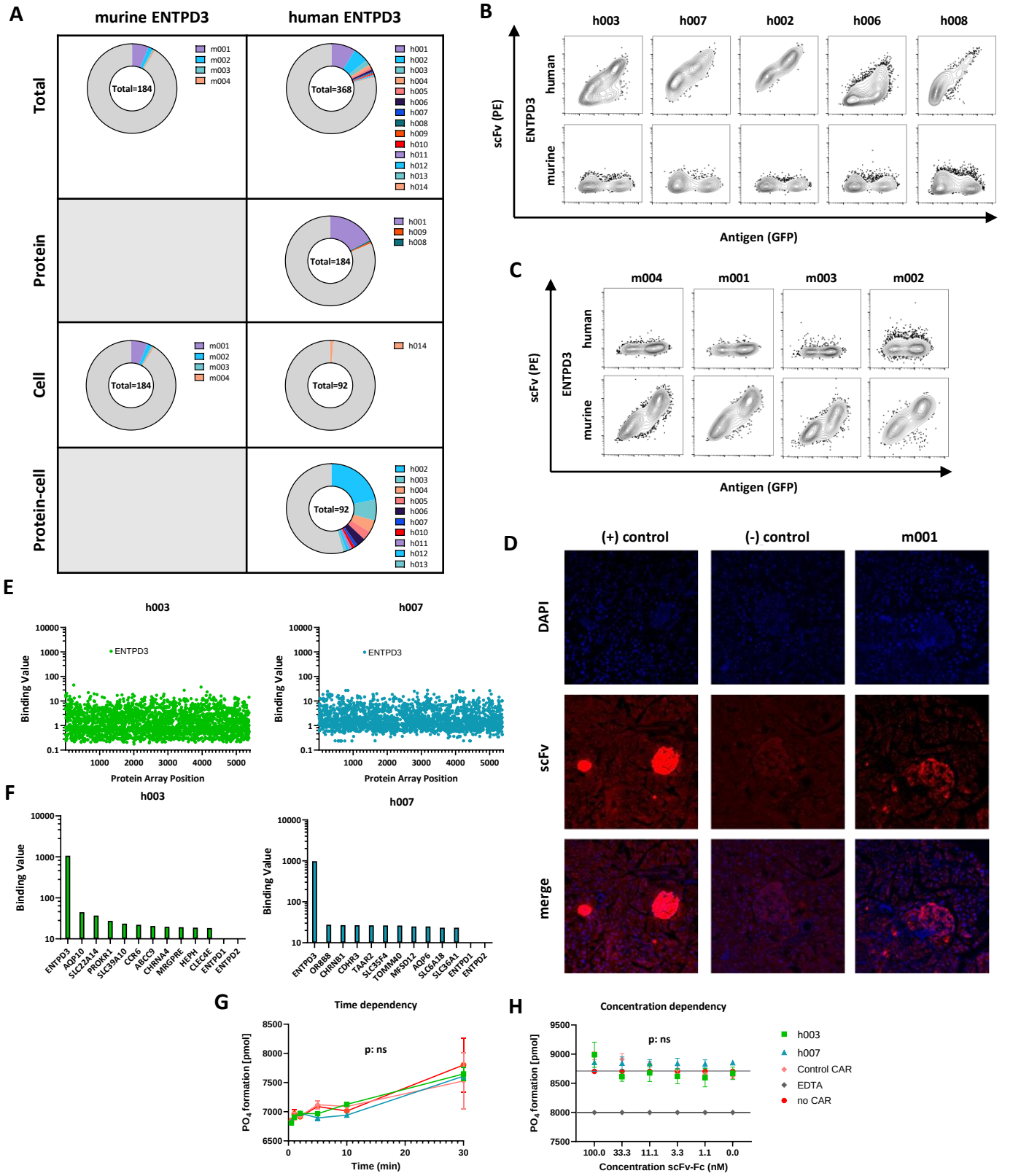

Figure 2: *Generation of ENTPD3-specific scFv binders by protein- and cell-based phage display* **(A)** Outcome of scFv binders by different panning strategies for murine ENTPD3 and human ENTPD3. Total number of analysed scFv binders per strategy are given in the centre of each plot. Proportions of unique scFv clones (color-coded) and non- and unspecific binders (grey). **(B-C)** Binding of human (B) and murine (C) ENTPD3-specific scFv binders was measured by flow cytometry on human or murine ENTPD3 expressing HEK293T cells, respectively. ENTPD3 expression on HEK cells was reported by coexpression of eGFP. Representative plots of selected binders. **(D)** Staining of C57BL/6 pancreatic sections by murine ENTPD3-specific binder m001. Insulin-specific FITC-conjugated antibody was used as positive control (left). Incubation with scFv m001 was followed by FITC-conjugated secondary antibody (right). Staining only secondary antibody served as negative control (middle). **(E)** Membrane Proteome Array (MPA) screening was performed by testing of human ENTPD3 binders. Binding values are given for clones h003 and h007 in an scFv-Fc format for 5,372 distinct human membrane protein clones. **(F)** Binding values of MPA for ENTPD3 and 10 following proteins with highest values and ENTPD1 and ENTPD2. **(G-H)** ENTPD3 enzymatic activity in the presence of soluble ENTPD3, ADP and scFv-Fc of h003 or h007. ENTPD3 activity (PO_4 formation) was measured by malachite green phosphate assay. Measured in triplicates. (G) Phosphate formation up top 30 min after incubation with 3.3 nM ENTPD3-specific scFv-Fc. No CAR and control CAR served as control. (H) Phosphate formation after incubation with varying concentrations (100 – 1 nM) of ENTPD3-specific scFv-Fc. Additionally, incubation with EDTA served as positive control for ENTPD3 inhibition. Data are presented as mean ± SD of triplicates. p values determined by two-way ANOVA of h003, h007 and Control CAR conditions, respectively. ns: $P > 0.05$.

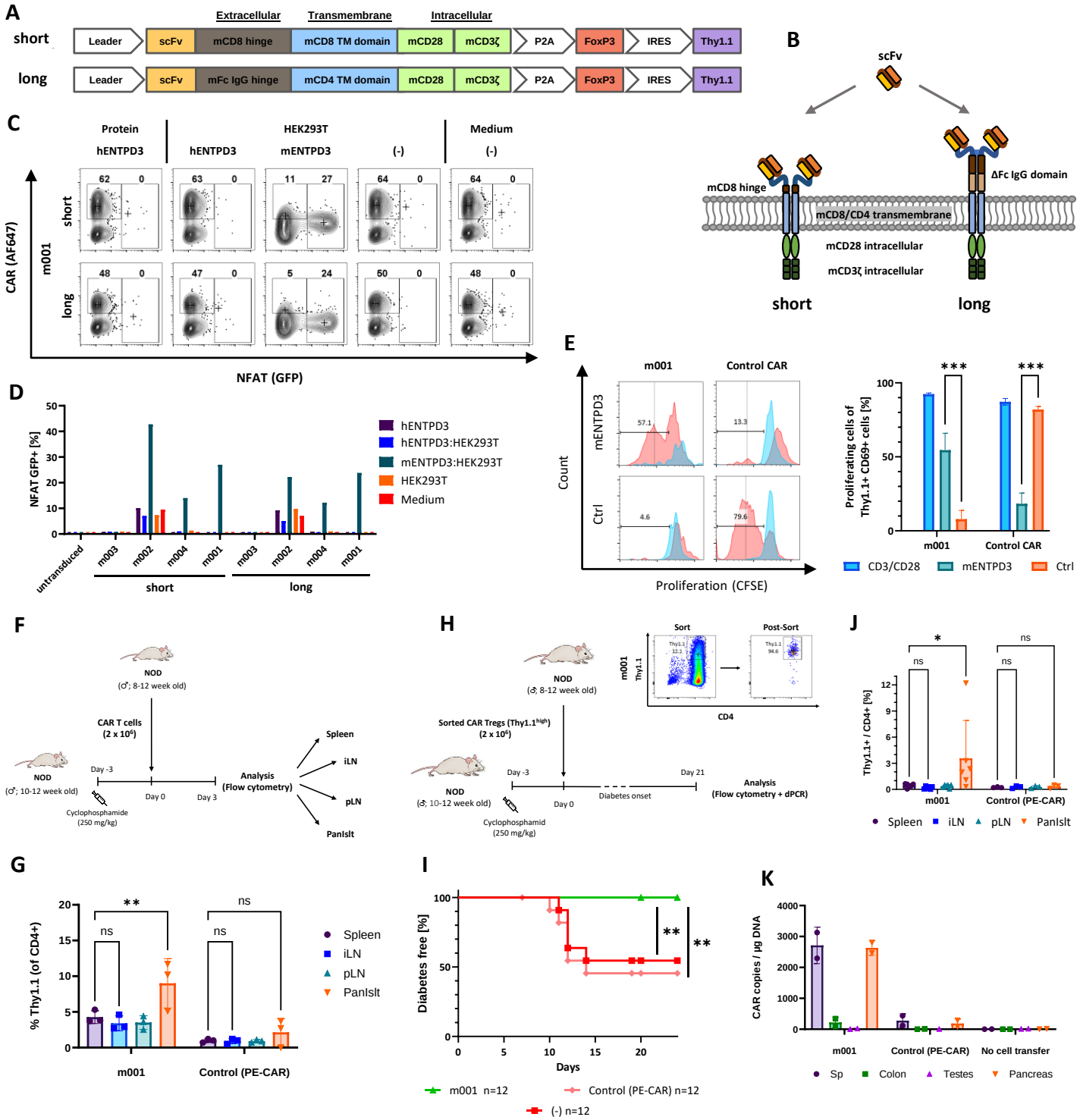

Figure 3: *Murine ENTPD3-specific CAR are functionally stimulated upon target contact and prevent cyclophosphamide-induced diabetes in vivo* **(A)** Design of murine CD8-derived hinge CARs (short) and Fc-IgG-derived hinge CARs (long), containing a FOXP3 expression cassette separated by P2A cleavage side, and reporter gene Thy1.1 (CD90.1) under control of an IRES. **(B)** Illustration of both CAR constructs as expressed on the cell surface. **(C)** Representative plots of stimulation of m001 in short and long hinge CAR format, respectively, in NFAT:GFP reporter cell line. CAR stimulation shown as NFAT-controlled GFP expression and CAR expression shown as anti-Fab antibody AF647 staining. **(D)** Screening of further murine ENTPD-specific candidates for CAR stimulation in the forementioned system. **(E)** Proliferation of CAR T cells measured as dilution of CFSE signal. CFSE labelled murine CD4+ CAR T cells (mL-m001 or Control (PE-specific) CAR) were stimulated on mENTPD3 or control antigen PE, or by aCD3/CD28 bead stimulus. Counts normalized to mode. Red: Stimulated CAR T cells (of CD69+ Thy1.1+). Blue: Unstimulated cells (of CD69- Thy1.1-). Left: Representative histograms. Right: Quantification of % Proliferation of stimulated CAR T cells (of CD69+ Thy1.1+). Mean ± SD, triplicates. p values determined by two-way ANOVA and multiple comparison testing (Tukey's test). **(F)** Schematic overview of setup for CAR T cell homing experiment in NOD mice. **(G)** Comparison of biodistribution of m001 and Control (PE-specific) CAR Teffs. CD4+ populations were analysed for percentage of Thy1.1+ cells. Data are presented as mean ± SD. n=3 per group. p values determined by two-way ANOVA and multiple comparison testing (Tukey's test). **(H)** Schematic overview of experimental setup for prevention of cyclophosphamide-induced diabetes in NOD mice. **(I)** Diabetes-free individuals over the course of the experiment. n=12 per group. Data from 8 independent experiments. p value determined by log-rank test for m001 CAR cTreg compared to Control (PE-specific) CAR cTreg and cyclophosphamide-only treated animals. **(J)** Comparison of biodistribution of m001 CAR-cTregs and Control (PE-specific) CAR cTregs at experimental endpoints (n = 3-6 per group). Data are presented as mean ± SD of Thy1.1+ in the CD4+ population. p values determined by two-way ANOVA and multiple comparison testing (Tukey's test). **(K)** Biodistribution of m001 CAR Tregs in ENTPD3-expressing tissues by digital PCR. Organs of two mice per group were saved at experimental endpoints and total gDNA was analysed by digital PCR. Copy numbers of CAR Treg-specific WPRE sequence per µg gDNA are displayed. P values for all experiments * P < 0.033, ** P < 0.002, *** P < 0.001.

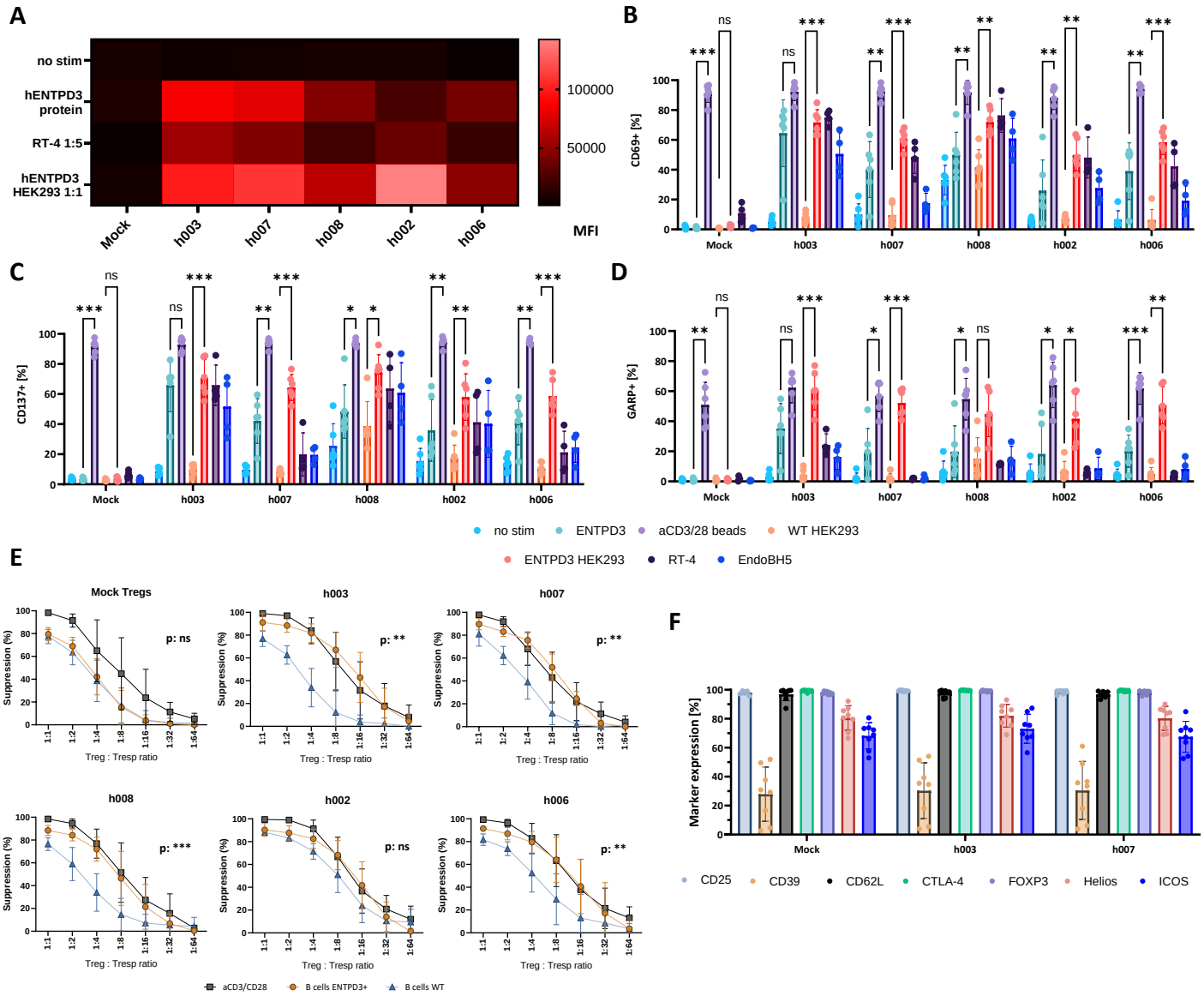

Figure 4: *Human ENTPD3-specific CAR Tregs are functional and maintain Treg phenotype and suppressive function* **(A)** NFAT luciferase Jurkat cell line was transduced with CARs comprising different human ENTPD3-specific scFv (h003, h007, h008, h002 and h006). After 5 days cells were activated with human ENTPD3 extracellular domain peptide, cell lines expressing ENTPD3 (RT-4 and ENTPD3.HEK293T) at indicated ratios or left unstimulated. Activation of cells was determined by luminescence measurement. Heatmap shows relative activation levels in response to stimulus. Black represents the lowest levels of activation with red/pink showing highest levels of activation. Representative of 3 separate experiments. **(B-D)** Human ENTPD3 CAR Tregs were co-cultured with ENTPD3 extracellular domain, ENTPD3 expressing HEK293T cells, RT-4, EndoBH5 cells or controls (aCD3/aCD28 beads, WT HEK293T and no stimulation). After 24h activation markers CD69 (B), CD137 (C) and GARP (D) were assessed by flow cytometry. Mean ± SD of n=6 donors. p values determined by two-way ANOVA and multiple comparison testing (Tukey's test). **(E)** Rested CAR Tregs were co-cultured with WT B cell line, ENTPD3 expressing B cell line or aCD3/28 beads and decreasing numbers of CTV-labelled CD4+ Teffs for 5 days. Cells were assayed by flow cytometry and proliferation was determined by CTV dilution. Graphs show percentage suppression of ENTPD3 CARs and mock transduced cells. Percentage suppression was calculated by normalizing proliferation of Teffs stimulated in the presence of Tregs to Teffs alone. Data are presented as mean ± SD of n=4-5 donors. p values determined by two-way ANOVA of B cells ENTPD3 and B cells WT conditions, respectively. **(F)** At day 14 of expansion h003 and h007 CAR Tregs were collected and stained by flow cytometry for indicated markers. Percentage of each marker shown from the total CD4 population for Mock Tregs or gated on CAR+ cells for the CAR Tregs. Mean ± SD of n=8 donors. P values for all experiments * P < 0.033, ** P < 0.002, *** P < 0.001.

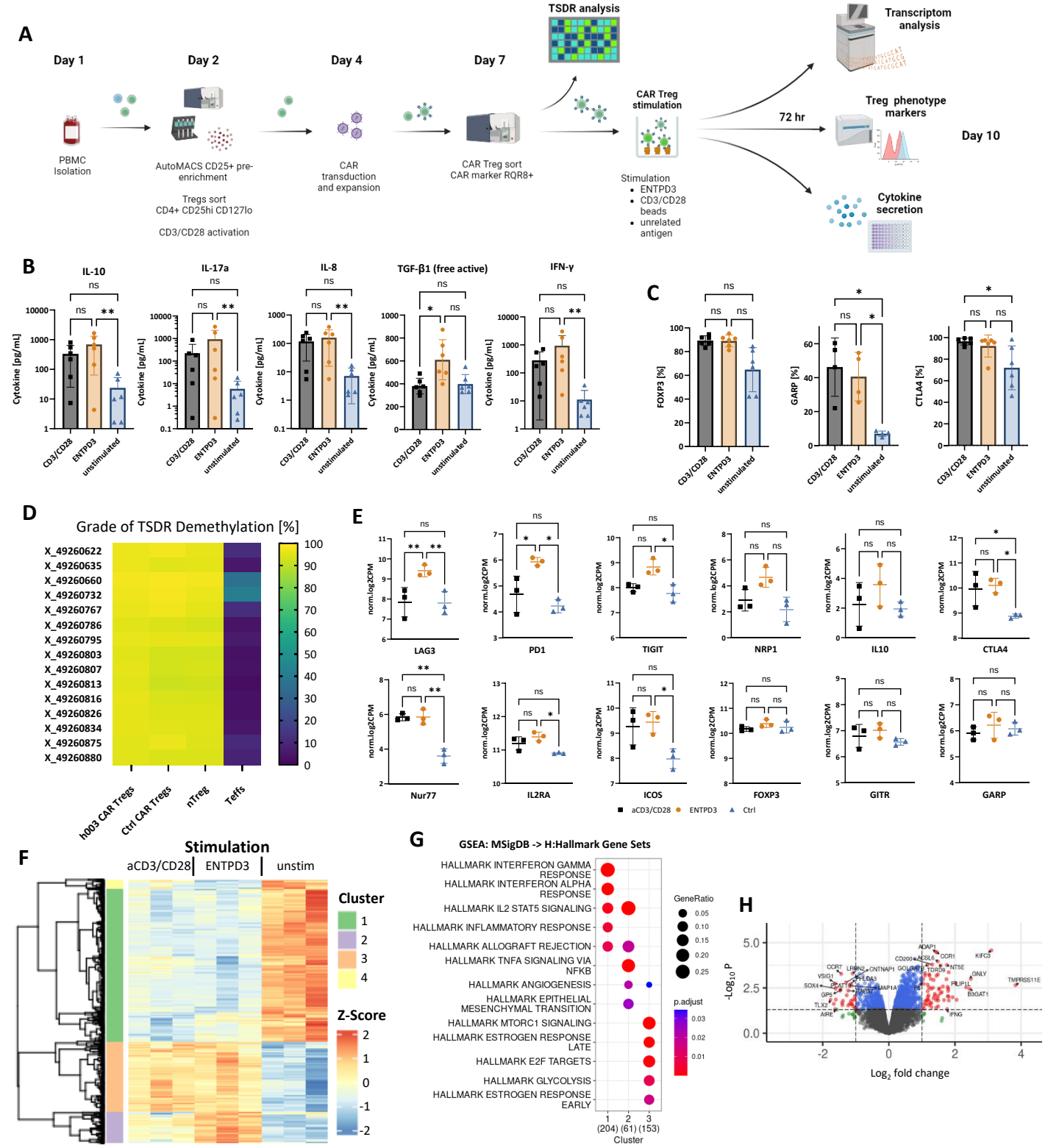

Figure 5. *ENTPD3 CAR Tregs (candidate h003) maintain Treg-specific phenotype and gene expression upon stimulation* **(A)** Schematic overview and design of human CAR Treg stimulation assay containing TSDR, transcriptomics and phenotype markers and cytokine secretion readouts for testing of CAR h003. **(B)** Treg cytokine profile upon CAR and TCR-dependent stimulation. ENTPD3 CAR Treg cells were incubated with ENTPD3, PE (control antigen) or aCD3/CD28 beads. Cytokine concentration was determined by cytokine bead array. Data are presented as mean ± SD of n=6 donors. p values determined by two-way ANOVA and multiple comparison testing (Tukey's test). **(C)** Expression of Treg phenotype and activation markers FOXP3, GARP and CTLA4 upon stimulation measured by flow cytometry. ENTPD3-specific h003 CAR Tregs stimulated by aCD3/CD28 beads (black), ENTPD3 (orange) or unrelated control antigen (blue). Data presented as mean ± SD of 4-6 donors. p values determined by two-way ANOVA and multiple comparison testing (Tukey's test). **(D)** Analysis of demethylation status of Treg-specific demethylated regions (TSDR). Percentage of demethylation of different TSDRs is shown for ENTPD3 CAR Tregs (h003), Control (PE-specific) CAR Tregs, nTregs and Teffs. Mean of data from 3 donors. **(E)** Gene expression of Treg phenotype and activation genes upon stimulation of h003 CAR Tregs measured by RNA Sequencing. Black: TCR-dependent stimulation by aCD3/CD28 beads. Orange: CAR-specific stimulation by ENTPD3. Blue: Unrelated control antigen. Data mean ± SD of 3 donors. p values determined by two-way ANOVA and multiple comparison testing (Tukey's test). **(F)** Cluster analysis of transcriptome data. Z-score (color coded) shown for TCR-dependent stimulation by aCD3/CD28 beads, CAR-specific stimulation by ENTPD3 and unstimulated (unrelated control antigen). Data of 3 donors per condition. **(G)** Analysis of Human Molecular Signatures Database (MSigDB) Hallmark gene sets of major clusters 1, 2 and 3. Size of dots represent ratio of represented genes within each cluster. P value is color coded. **(H)** Volcano plot of differentially expressed genes in pairwise comparison of CAR- (ENTPD3) and TCR- (aCD3/CD28 beads) specific stimulation. P values for all experiments * P < 0.033, ** P < 0.002, *** P < 0.001.

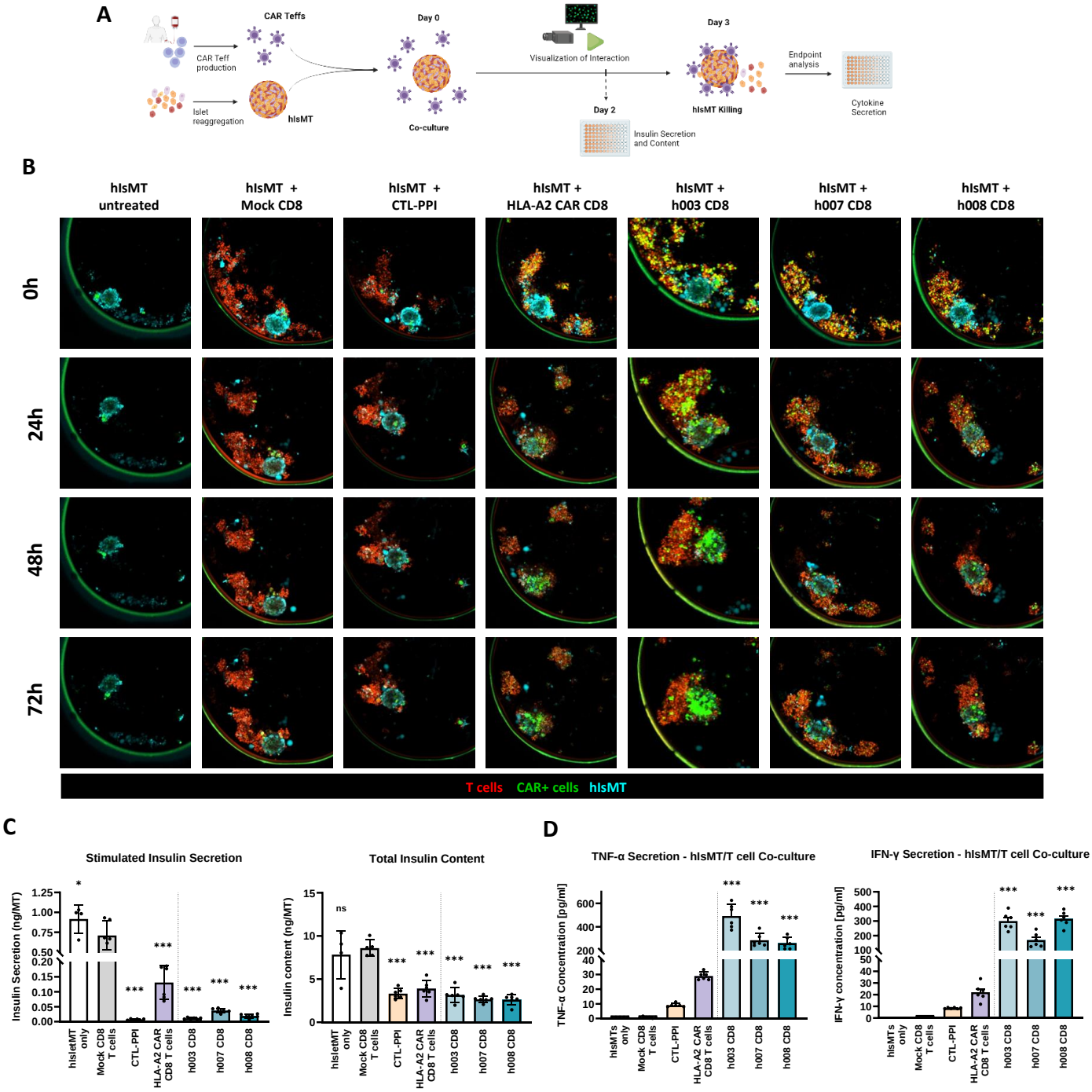

Figure 6: *ENTPD3-specific CARs interact with human islets micro tissue (hIsMT) spheroids* **(A)** Schematic assay setup. **(B)** Human CD8+ T cells expressing either ENTPD3 CARs (h003, h007 or h008) or HLA-A2 CAR, and GFP reporter cassette were co-cultured with hIsMT spheroids for live imaging. Images show the hIsMT alone, with non-transduced CD8 T cells (Mock), preproinsulin (PPI) specific cytotoxic lymphocytes (CTLs) or CD8 T cells expressing HLA-A2 CAR or ENTPD3 CARs h003, h007 or h008 for timepoints 0, 24, 48 and 72 h. T cells are shown in red, CAR expression is shown in green and hIsMT are stained cyan. **(C)** After 48 h samples of co-cultures were lysed and stimulated insulin secretion (left) and total content (right) was determined by ELISA. Individual dots are technical replicates. Bars represent mean ± SD of n=4-6 **(D)** After 72 h supernatants were collected and assayed for IFN-γ (left) and TNF-α (right). Individual dots are technical replicates. Bars represent mean ± SD of n=6. p values determined by One-way ANOVA with Dunnett's multiple comparisons test comparing all conditions to mock CD8 T cells. Outliers were be detected with ROUT's outlier test (Q=5%). *p < 0.05, **p < 0.01, ***p < 0.001.